Desalination and Water Treatment
www.deswater.com

doi: 10.5004/dwt.2018.21858

104 (2018) 241–249
February

Photocatalytic degradation of TNT in wastewater using Fe-doped TiO_2 nanoparticles

Sahar M. Ahmed, Seham A. Shaban*, Doaa S. El-Desouki, Noha A.K. Aboul-Gheit, Samira M. Abdel-Azim

Catalysts Characterization Laboratory, Petroleum Refining Division, Egyptian Petroleum Research Institute (EPRI), 1 Ahmed El Zomour St., Nasr City, PO Box 11727, Cairo, Egypt, Tel. +20 2 22736349; Fax +20 2 22747433; emails: sehamshaban@yahoo.com (S.A. Shaban), saharahmed92@hotmail.com (S.M. Ahmed), doaadesouki@hotmail.com (D.S. El-Desouki), nohaaboulgheit@yahoo.com (N.A.K. Aboul-Gheit), samiraepri@hotmail.com (S.M. Abdel-Azim)

Received 20 August 2016; Accepted 24 December 2017

ABSTRACT

Titanium(IV) oxide powders doped with nanocrystalline iron were synthesized by a sol–gel method. The function of iron is twofold: (i) it serves to improve the absorption of photons by TiO_2 and (ii) it inhibits the recombination of electron–hole pairs in excited states. Iron content varies from 0 to 0.8 wt% of the powders being prepared. The surface morphology, phase transformation, surface characteristics and absorption bands of the nanoparticles prepared for this exercise were examined. The physico-chemical properties of the nanoparticles prepared for the prepared catalysts were examined by special instrumental analytical methods: transmission electron microscopy for the surface morphology, X-ray diffraction for the phase transformation, Brunauer–Emmett–Teller for surface characterization and UV–visible spectroscopy for determination of absorption bands. The phase transformation of TiO_2 from anatase to rutile was catalyzed by iron. It was observed that: (i) the grain size of TiO_2 decreased with increasing iron content; (ii) the surface area of catalysts increased with increasing iron(III) oxide loading, up to 0.6 wt%; (iii) beyond 0.6 wt%, the surface area decreased with increasing iron content and (iv) the rate of photocatalytic degradation of trinitrotoluene was optimal at an iron content of 0.6 wt%.

Keywords: Degradation; Nanoparticles; Photocatalytic; TNT

1. Introduction

Transition metal doped TiO_2 is regarded as an efficient photocatalyst, because addition of transition metal ions increases the optical absorption towards the visible light region and decreases the band gap comparing with that of pure TiO_2 (3.1 eV). The large absorptive areas in the solid matrix of TiO_2 may be due to charge transfer from the 3d orbitals of the transition metal ions to the TiO_2 conduction band [1–5]. Several published literatures have studied the effect of transition metal ions in TiO_2. Ola and Maroto-Valer [2] reported that, the incorporation of V, Cr and Co ions in TiO_2 matrix resulted in a red shift of the absorption which was due to defect centers created by the substitution of Ti^{4+} with metal ions.

Furthermore, an appropriate amount of doped ions of TiO_2 can inhibit electron–hole recombination and narrow its band gap, remarkably improving the photocatalytic activity of TiO_2. Fe^{3+} has been proved to be a successful dopant ion due to its stable half-filled electronic configuration [2,6]. According to the crystal field theory, Fe^{3+} has a valence electronic configuration of $3d^5$. When these ions trap electron/hole, the spin states change from high spin of five unpaired electrons to low spin of four unpaired electrons. The trapped electron/hole will be transferred to surface adsorbed water molecules to restore its spin energy, there by inhibiting the recombination

* Corresponding author.

of photogenerated electron–hole pairs. This inhibition in the recombination rate of electron–hole pairs increases the life time of the catalyst. A lot of research has been carried out to investigate the photocatalytic properties of doped TiO_2. A great variety of organic and inorganic pollutants [7–12] were decomposed by redox reactions on the surfaces of these catalysts. In addition, trinitrotoluene (TNT) and TiO_2 absorb only UV light because their band gap energy is too high. In order to improve its ability of absorption, visible light sanitization of TNT has been studied extensively [13]. In heterogeneous photocatalysis, certain metal oxides in water upon adsorption of UV radiation, readily generate hydroxyl radicals which are the most reactive species having the highest oxidation potential for breaking complex organic bonds [14]. These metal oxides are semiconductors and used as photocatalysts. Electrons in the photocatalyst are promoted from the valence band to the conduction band, producing electron–hole pairs [15]:

$$A_{\text{ground state}} + h\nu \rightarrow A_{\text{excited state}} \quad (1)$$

where e^-_{cb} and h^+_{vb} are the electrons in the conduction band and the electron vacancy in the valence band, respectively. The electron–hole pair then moves up to the catalyst surface, where it can enter into a redox reaction with other species on the catalyst surface. In aqueous media, h^+_{vb} reacts with surface bound H_2O to produce $^{\bullet}OH$ radicals, whereas e^-_{cb} reacts with O_2 to produce superoxide radical anion of oxygen. As such, photocatalytic reaction is said to be a surface phenomenon.

$$H_2O + h^+_{vb} \rightarrow {}^{\bullet}OH + H^+ \quad (2)$$

$$O_2 + e^-_{cb} \rightarrow {}^{\bullet}O_2^- \quad (3)$$

The above redox reaction prevents the recombination of the electron–hole pair produced in Eq. (1). The $^{\bullet}OH$ radical also reacts with water to form more $^{\bullet}OH$ radicals, as seen in the Eqs. (4) and (5). The $^{\bullet}OH$ radicals and O_2^- anion produced in Eqs. (2)–(5) then react with the TNT to break it down into innocuous end products (Eqs. (6) and (7)).

$$2[O^{\bullet}{}_2]^- + 2H^+ \rightarrow H_2O_2 + O_2 \quad (4)$$

$$2H_2O_2 \rightarrow 2{}^{\bullet}OH \quad (5)$$

$${}^{\bullet}OH + TNT \rightarrow TNT_{\text{oxidized}} \quad (6)$$

$$TNT + e^-_{cb} \rightarrow TNT_{\text{reduced}} \quad (7)$$

Finally, when titanium dioxide (TiO_2) is illuminated with light of band gap energy, electrons in conduction band (e^-_{cb}) and holes in valence band (h^+_{vb}) are produced according to Eq. (1). These charge carries can recombine, or the holes can be scavenged by oxidizing species (e.g., H_2O, ^-OH), and electron by reducible species (e.g., O_2). The hydroxyl radical is a highly reactive oxidizing reagent and can decompose most organic contaminants (Eqs. (8) and (9)).

$$h^+_{vb} + {}^{\bullet}OH \rightarrow {}^{\bullet}OH \quad (8)$$

$$e^-_{cb} + O_2 \rightarrow {}^{\bullet}O_2^- \quad (9)$$

As a photocatalyst functioning in diverse chemical environments of wastewaters, TiO_2 has certain advantages besides its favorable band gap energy and catalytic efficiency. The structural integrity of the solid matrix is evinced by its insolubility and resistance to chemical and biological attacks. TiO_2 is non-toxic and can be obtained commercially at low cost [16]. These factors have combined to make TiO_2 a successful photocatalyst for the degradation of pollutants [17]. It has been reported that the addition of Pt [18], Cr^{3+} [19], Cu^{2+} [20], Fe^{3+} [21–26] or other cations into anatase titania can improve its photoactivity. Among them, Fe-doped TiO_2 system is considered as a potential candidate for photocatalyst, and it has been reported that the photocatalyst improved with optimal Fe content [21,23]. Various methods have been used to synthesize Fe-doped TiO_2 nanoparticles, such as sol–gel method [24], impregnation [23] and hydrothermal method [21,25,26].

In this paper, preparation of TiO_2 mixed oxides by sol–gel method in different molar ratios of Fe_2O_3/TiO_2, and their catalytic activities were tested for the degradation of wastewater containing TNT coming from Military Factory (Abou Zaabal Co., for specialized chemicals F/18).

2. Experimental

2.1. Materials

All chemicals used in this study were analytical grade reagents.

2.1.1. Physical characterization of the prepared catalysts

Identification of the prepared catalysts was examined by powder X-ray diffraction (XRD) diffraction analysis using analytical X-ray diffractometer, Cu Kα radiation of wavelength λ = 1.5406 Å, rating of 40 kV, 40 mA, step size = 0.02, and scan step time of 0.4 s in the 2θ range 10–80.

The morphology of the samples was examined by transmission electron microscopy (TEM; Tokyo, Japan) on a JEOL JEM-2000EX (Tokyo, Japan) at an accelerating voltage of 100 kV and scanning electron microscopy (SEM). The emission SEM (Tokyo, Japan) was performed with a JEOL 5400 (Tokyo, Japan).

The surface area was determined from nitrogen adsorption–desorption isotherms at liquid nitrogen temperature (77 K) using a Quantachrome AS1W in version 2.01 instrument. The samples were outgassed for 3 h at 150°C. The Brunauer–Emmett–Teller (BET) method was used for surface area calculation, while pore-size distribution (pore diameter and volume) was determined by the Barrett–Joyner–Halenda method.

Diffuse reflectance spectroscopy and visible-ultraviolet spectra were obtained by diffuse reflectance spectroscopy using a Shimadzu UV-2401 PC instrument. $BaSO_4$ was the reference sample and the spectra were recorded in the range 200–800 nm.

For photocatalytic activity measurement, high performance liquid chromatography (HPLC) using HPLC Waters 600 apparatus, equipped with an auto sampler (Waters 717 plus) and a dual wavelength absorbance diode array detector (Waters 4487) set at 254 nm was used with C18 5 μm, 4.6 mm × 250 mm column (part no. 186004117) purchased

from Water, USA. The mobile phase was HPLC grade water/acetonitrile (30/70) operating at a rate of 1 cm^3/min a 100 ppm TNT standard stock solution. Dilutions of these stock standards were made to give 90–10 ppm TNT standards. These standards were then injected into the HPLC for each TNT kinetic run, and a calibration curve was thus obtained.

2.2. Preparation of photocatalysts

The mixed oxides were prepared by the sol–gel technique using titanium isopropoxide and Fe(III) acetylacetonate as Ti and Fe precursors, respectively. In a typical preparation, Ti isopropoxide was added dropwise to the solution of propanol and HNO_3 at room temperature with constant stirring. Fe(III) acetylacetonate was similarly dissolved in propanol then mixed with the solution of Ti isopropoxide with vigorous stirring. The prepared sol was left to stand and form gel, which was aged for 5 d at room temperature then calcined at 550°C for 5 h. (Table 1) The TNT samples were collected from Military Factory (Abou Zaabal Co., for specialized chemicals F/18).

2.3. Photocatalytic activity experiments

A quartz photoreactor was used in this study, in which tungsten halogen lamp with an emission of λ (300–800) nm was positioned inside the cylindrical quartz vessel surrounded by a circulating water jacket (quartz) for cooling as shown in Scheme 1. The photodegradation experiments were carried out by dissolving TNT in deionized water at the desired concentration 1×10^{-4} mol/dm^3. The catalyst loading was 0.5 g/L and appropriate quantities of the suspensions (500 mL) were magnetically stirred in the dark for 30 min to reach an adsorption/desorption equilibrium between the photocatalyst and TNT. All experiments were performed at 25°C ± 1°C at pH 7. In order to remove photocatalyst particles before analyses, samples were filtered through 0.45 μm pore size cellulose acetate filters. The concentration of the TNT was analyzed by HPLC (Fig. 1) [27–30].

Table 1
Crystal size of pure TiO_2 and Fe(III) incorporated TiO_2 catalysts at different loading

Sample	Fe(III) loading (%)	Crystal size (nm) from XRD
I	0	47.4
II	0.2	29.5
III	0.4	49.9
IV	0.5	27.2
V	0.6	20.5
VI	0.8	24.7

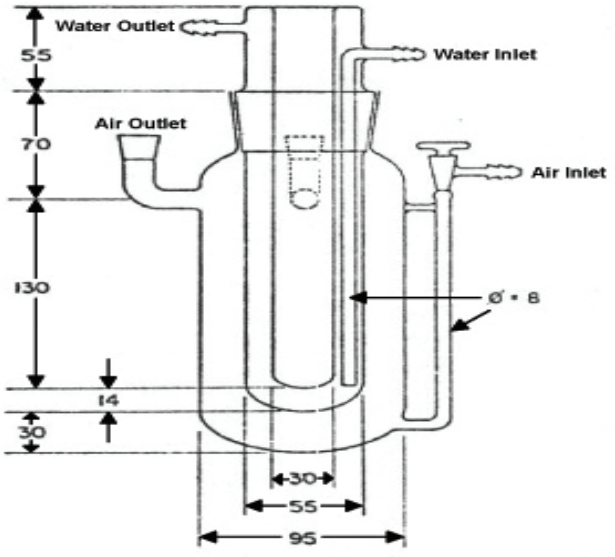

Fig. 1. Quartz photoreactor [29].

3. Results and discussion

3.1. X-ray diffraction

Fig. 2 represents the XRD pattern used for the current mixed oxides calcined at 550°C for 5 h in air. It is observed that all catalysts obtained at different TiO_2/Fe_2O_3 molar ratios of mixed oxides contain both anatase and rutile phases. The XRD pattern for sample I (TiO_2 prepared under similar conditions and heat treated at 550°C) consists of very sharp peaks of the anatase phase with no indication of the presence of rutile phase. The mass fraction of anatase and rutile is calculated from the (101) reflection of anatase at 2θ = 25.48° and the (110) reflection of rutile at 2θ = 27.5°. The crystallite size of these phases calculated applying Scherer's equation $D = 0.9\lambda/\beta\cos\theta$, where D is the thickness of crystallite, λ is X-ray wavelength, β is full width at half maximum and θ is Bragg's angle (Table 1).

All diffractograms show the presence of tetragonal titania with no iron containing phases. Therefore, the formation of mixed phases at 550°C can be attributed to the fact that the presence of iron may have catalyzed the transformation of anatase phase to rutile phase. These results are also supported by the reported data given by Aboul-Gheit et al. [30]. As can be seen from the XRD patterns samples II, III and VI have peaks of rutile stabilized. In fact, as the Fe^{3+} (0.55 Å) radius is

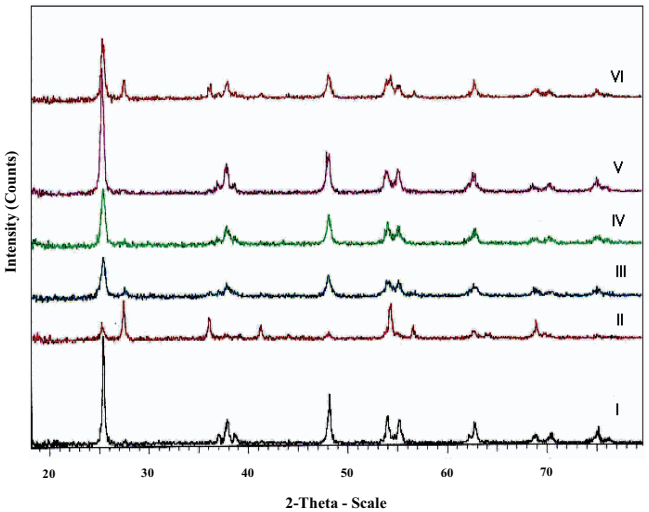

Fig. 2. XRD patterns of the mixed oxides.

almost equal to that of Ti^{4+} (0.605 Å) [31], the substitution of iron in the matrix of TiO_2 is a favorable process and easier in rutile due to the open channels present in this structure. Many reports about the structural studies of Fe(III)/TiO_2 system [32] have revealed that Fe^{3+} enters the TiO_2 lattice substitution. During the preparation of mixed oxides by sol–gel process, titanium alkoxide hydrolysis quickly to Ti hydroxide and Fe(III)–acetylacetonate remained as it is because its hydrolysis requires drastic reflusking with an organic base like sodium ethoxide. Therefore, in the mixed sol, TiO_2 was coated completely with Fe(III) acetylacetonate complex [33]. During heat treatment at 550°C, the preadsorbed Fe precursor decomposes to Fe_2O_3 from which a certain fraction enters into the TiO_2 lattice. However, the XRD data does not show the presence of Fe_2O_3 particles in the mixed oxide system. XRD data are not particularly sensitive to the distribution of Ti and Fe in oxides. Since X-rays are scattered by electron density, and since Ti and Fe are surrounded by approximately the same number of electrons, they are difficult to accurately distinguish in an XRD experiment [34].

3.2. FTIR spectra of mixed oxides samples

Fig. 3 shows that pure TiO_2 spectrum (I) is similar to the other mixed oxides (for samples II–VI) which were doped with different ratios of Fe_2O_3 all samples show absorption band at 871 cm^{-1} of TiO_2 anatase and their small peaks are around 1,625, 1,492 and 1,325 cm^{-1} for samples II, III and VI were detected. These peaks are attributed to the TiO_2 rutile phase. It is noticed that there are no obvious peaks for Fe_2O_3. This indirectly indicates that Fe_2O_3 is dissolved into the TiO_2 lattice and forms a solid solution. These results are in agreement with the XRD data. The IR stretching vibration occurring in the region 2,200–2,400 cm^{-1} can be attributed to CO molecules which adsorbed on the surface of the bimetallic nanoparticles. Toshima and Yonezawa [35] explained that IR spectroscopy of CO on the surface gave some information about the surface structure of bimetallic nanoparticles. By comparison of IR spectra of CO on a series of bimetallic nanoparticles at various metal compositions. Hence, the surface microstructure of bimetallic nanoparticles can be elucidated.

3.3. UV–Vis spectra

UV–Vis spectra of the prepared catalysts are shown in Fig. 4, where the increase of absorption at wavelength 280 cm^{-1} can be assigned to the absorption band of anatase TiO_2. The presence of iron gives absorption in the visible region below 400 nm which increases with increasing the iron content, in consistency with the changes in the color of the samples from white to yellow or light brown. The spectra of Fe-doped TiO_2 nanoparticles displayed a red shift in the band gap transition with the increase of Fe content. It has been reported that this shift resulted from the incorporation of iron ions into the TiO_2 nanoparticles prepared by the sol–gel method [36]. Red shifts of this type could be attributed to the excitation of 3d electrons of Fe(III) to the TiO_2 conduction band where the charge transfer gives rise to a band at 400 nm which enhances absorption in the visible region. It has been reported [22] that doping TiO_2 with transition metals extends the absorption of TiO_2 in the visible region of the solar spectrum [37–39].

3.4. Surface area and crystalline size

The influence of Fe(III) loading on the BET surface area, pore volume and pore-size distribution was investigated. Fig. 5 shows the N_2 adsorption–desorption isotherms of the pure TiO_2 and Fe(III)/TiO_2 powders prepared at different Fe(III) loadings ranging from 0 to 0.8%. It is noted that all catalysts displayed isotherms of type IV, signifying that the catalyst powder contained mesopores with sizes ranging from 2 to 50 nm. BET surface area, pore volume and average pore-size distribution of each catalyst are given in Table 2. It shows that an increase of Fe(III) loading initially led to an increase in the BET surface area of the catalyst. Pure TiO_2 had a surface area of 44.55 m^2/g and an incorporation of 0.6% of Fe(III) significantly increased the surface area to 112.17 m^2/g. However, a further increase of Fe(III) leads to reduction of the BET surface area from 112.17 to 48.58 m^2/g when Fe(III) loading was increased from 0.6% to 0.8%.

The average pore diameter of the catalysts is found to be in mesoporous size range (Table 2). The formation of

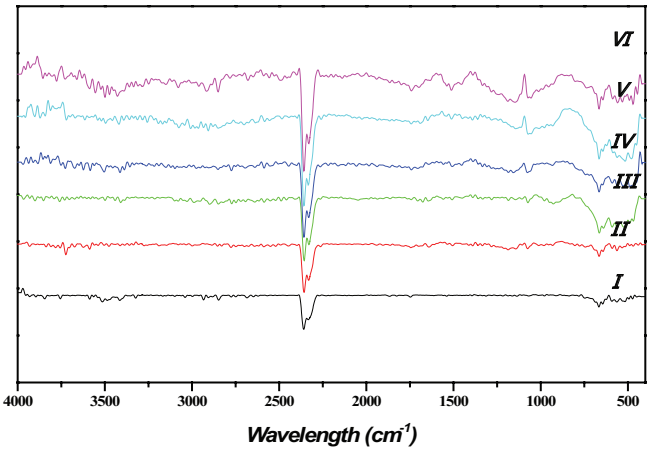

Fig. 3. FTIR spectra of the prepared catalysts.

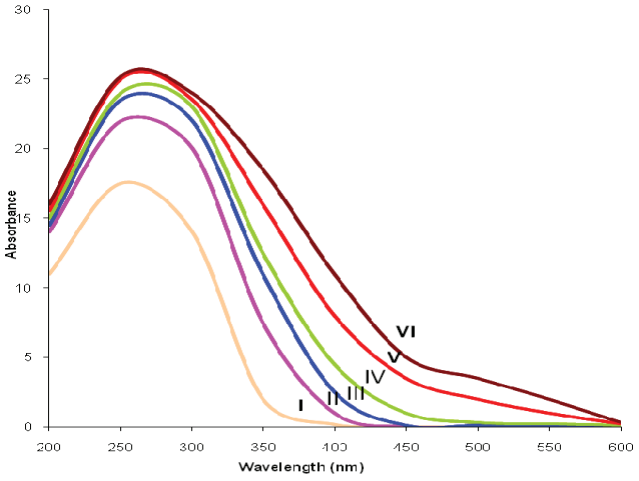

Fig. 4. UV–Vis spectra of the prepared nanocatalysts.

mesoporous structure in the prepared catalysts was attributed to the aggregation of TiO_2 crystallites [40]. Small mesopores are attributed to the finer intra-aggregated pores formed between TiO_2 grains or primary particles (represented by the hysteresis loop in the lower P/P_0 range from 0.4 to 0.7 in Fig. 5). Large mesopores are ascribed to the larger inter-aggregated pore (hysteresis loop in the higher P/P_0 range from 0.7 to 1.0). The results show that the addition of low loading of Fe(III) might prevent the pore walls from experiencing excessive collapse or distortion by limiting the grain growth during heating. This result may be helpful to explain the larger BET surface area and the more uniform pore distribution of Fe(III)-doped TiO_2 at 0.6% with an average pore diameter equal to 3.709 nm. A further increase of Fe(III) loading to 0.8% Fe(III) would lead to a decrease of average pore diameter to 1.65 nm. It was suggested that the incorporation of Fe(III) into TiO_2 could restrain the growth rate of the particles during heat treatment [41]. Thus, Fe(III)-doped TiO_2 possessed larger BET surface area and more uniform pore distribution as compared with the pure TiO_2. Therefore, the surface properties of the mesoporous catalyst would be improved with a suitable amount of Fe(III) ions loaded [42].

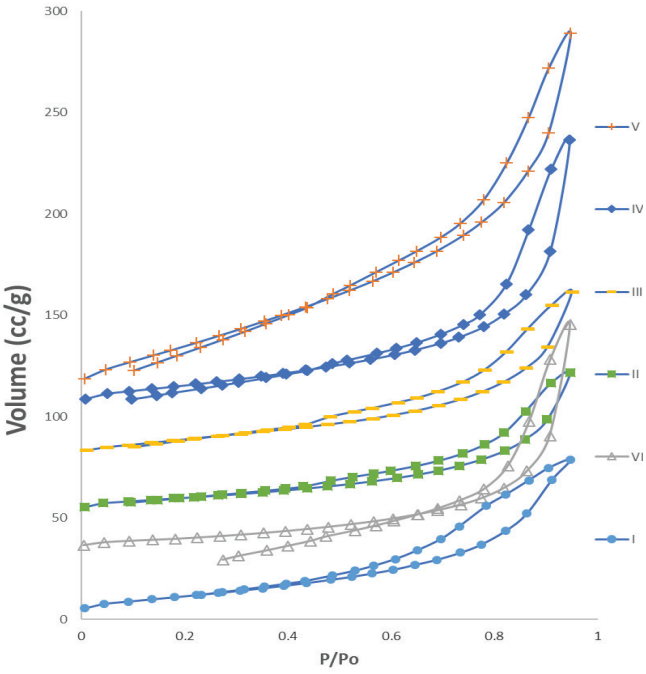

Fig. 5. N_2 adsorption–desorption isotherm of pure TiO_2 and Fe(III)/TiO_2 catalyst with different Fe(III) loading.

3.5. TEM studies

Surface morphology and distribution of particles are shown in the TEM image photograph. The TEM photographs of the samples heat treated at 550°C are shown in Fig. 6. It is clear that the samples have nanocyrstalline nature. The prepared nanoparticles of TiO_2 (sample I) was tetragonal, with diameters ranging from 30 to 50 nm, while samples II and III were more uniform semispherical with an average particle sizes of 15–30nm. The TEM of samples V and VI were

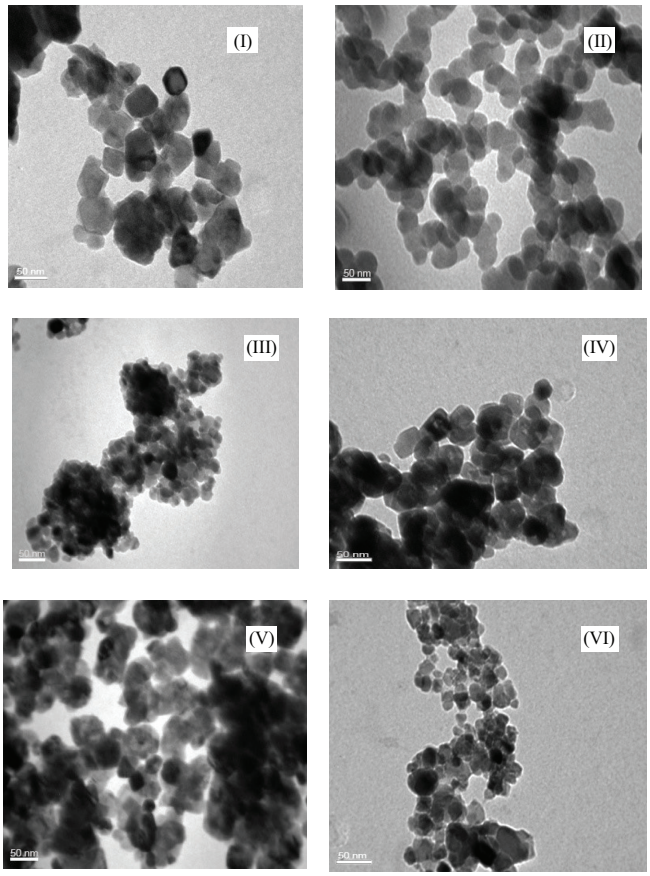

Fig. 6. TEM of mixed oxides.

Table 2
Properties of pure TiO_2 and Fe(III) incorporated TiO_2 catalyst at different loading

	Sample	Fe(III) loading (%)	Properties		
			BET surface area (S_{BET}, m^2/g)	Total pore volume (cm^3/g)	Average pore diameter (dp, nm)
I	Pure TiO_2	0	44.55	0.1220	7.443
II	0.2 Fe/TiO_2	0.2	51.21	0.2573	3.671
III	0.4 Fe/TiO_2	0.4	60.64	0.1567	3.712
IV	0.5 Fe/TiO_2	0.5	73.65	0.2691	3.709
V	0.6 Fe/TiO_2	0.6	112.17	0.2769	3.708
VI	0.8 Fe/TiO_2	0.8	48.58	0.1541	1.654

cubic-shaped with particle sizes ranging from 15 to 25 nm. These values are in good agreement with the XRD crystallite size results.

3.6. Photodegradation of TNT

The transition metal ion used as dopants enhances the attachments of the functionalized organic pollutants to the doping ion active sites [43].

It is very important to determine the mechanism of photosensitization and the recombination of excited electron–hole pairs affected by depositing transition metal oxide on the surface of TiO_2 to enhance the photocatalytic activity. To evaluate the photocatalytic activity of the mixed oxides and to determine the optimum content of Fe, the photodegradation characteristic of TNT over mixed oxide has been investigated. A suspension of the catalyst and pollutant in water was stirred in the dark for 30 min to reach adsorption equilibrium. The degree of degradation in the TNT concentration due to adsorption was about 2%–3%. The TNT photodegradation over mixed oxides is shown in Fig. 7. The rate constant of photodegradation of TNT increased with an increase in Fe(III) content at below 0.6 wt%, but it decreased with increasing Fe(III) content at above 0.6 wt%. This suggests that the optimum content of Fe(III) is 0.6 wt%. Choi et al. [44] proposed that it appeared to be an optimal dopant concentration, above which the observed photoactivity decreased. On the basis of the relevant band position of Fe(III) and TiO_2, Fe(III) clusters at lower wt% act as a separation center. The photogenerated electrons are transferred from TiO_2 to the Fe(III) conduction band and the holes accumulated in the TiO_2 valence band. Hence, photogenerated electrons and holes are efficiently separated. However, Fe(III) clusters at higher wt% act as a recombination center and the recombination rate between electrons and holes increase exponentially with increasing Fe(III) wt% because the average distance between trap sites decreases particle. Therefore, from data in Fig. 7 it can be concluded that Fe(III) doping on TiO_2 enhances the photocatalytic activity and an optimal content of 0.6 wt% Fe(III)/TiO_2 which leads to the best photocatalytic performance for TNT degradation. The enhancement in the photocatalytic degradation activity of various organic substrates upon iron doping of titania is in line with observations by Ranjit and Viswanathan [45]. It also can be proposed that iron doping, promotes phase transformations which modify electron–hole properties. Kokila et al. [46] had reported that the presence of metal ions on the surface of the photocatalyst particles improves the rate of electron transfer to O_2 and consequently has a beneficial effect on the photo-oxidation rate of organic species. The more number of pores increases the hydroxyl content. In heterogeneous photocatalysis, the illumination of semiconductor produces electrons (e^-) and holes (h^+). The holes (h^+) are combining with OH ions and there is formation of hydroxyl radicals ($h^+_{vb} + OH^- \rightarrow {}^{\bullet}OH$). These surface hydroxyl radicals formed on the surface of the photocatalyst are oxidizing species which ultimately affects the photocatalytic activity. Also stated that these dopants exist only as the recombination center for the electron/holes, thus having no noticeable effect on the reaction rate [47].

The reaction rate constants (k) of the prepared catalysts for photodegradation of TNT were calculated according to the following formula: $\ln(C_0/C_t) = kt$, where C_0 and C_t are the concentrations of TNT in the primary stage of experimental and after (t) minutes irradiation Fig. 8. As shown in Fig. 9, k first increases with increasing the Fe-doping concentration, then reaches to an optimum value when Fe-doping concentration is 0.6%. Further increasing the amount of Fe above

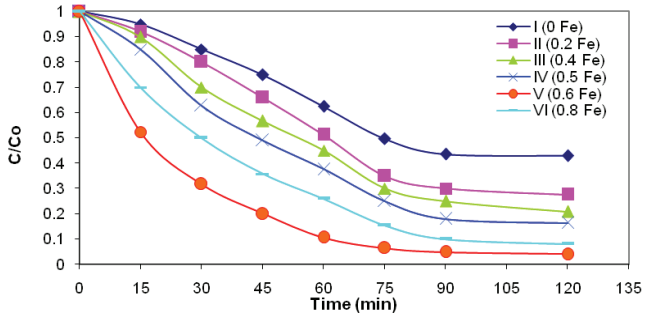

Fig. 7. Photocatalytic degradation of TNT using different mixed oxides.

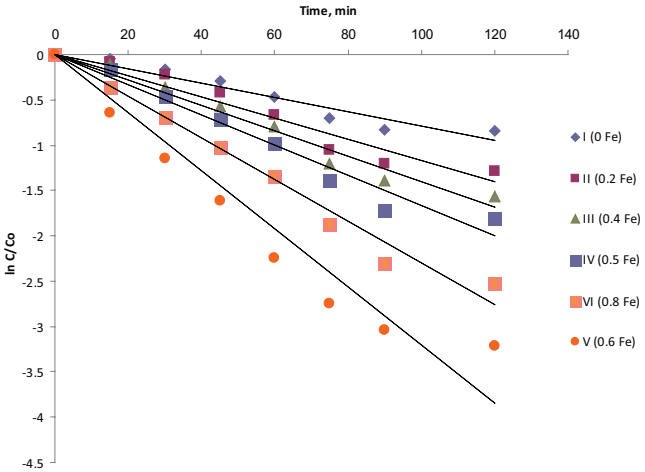

Fig. 8. Relationship between logarithmic plots of TNT concentration vs. time with different Fe-doped.

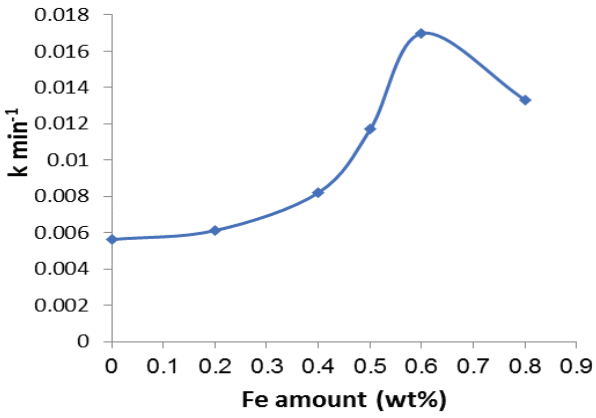

Fig. 9. Relationship of observed rate constant and concentration of Fe-doped.

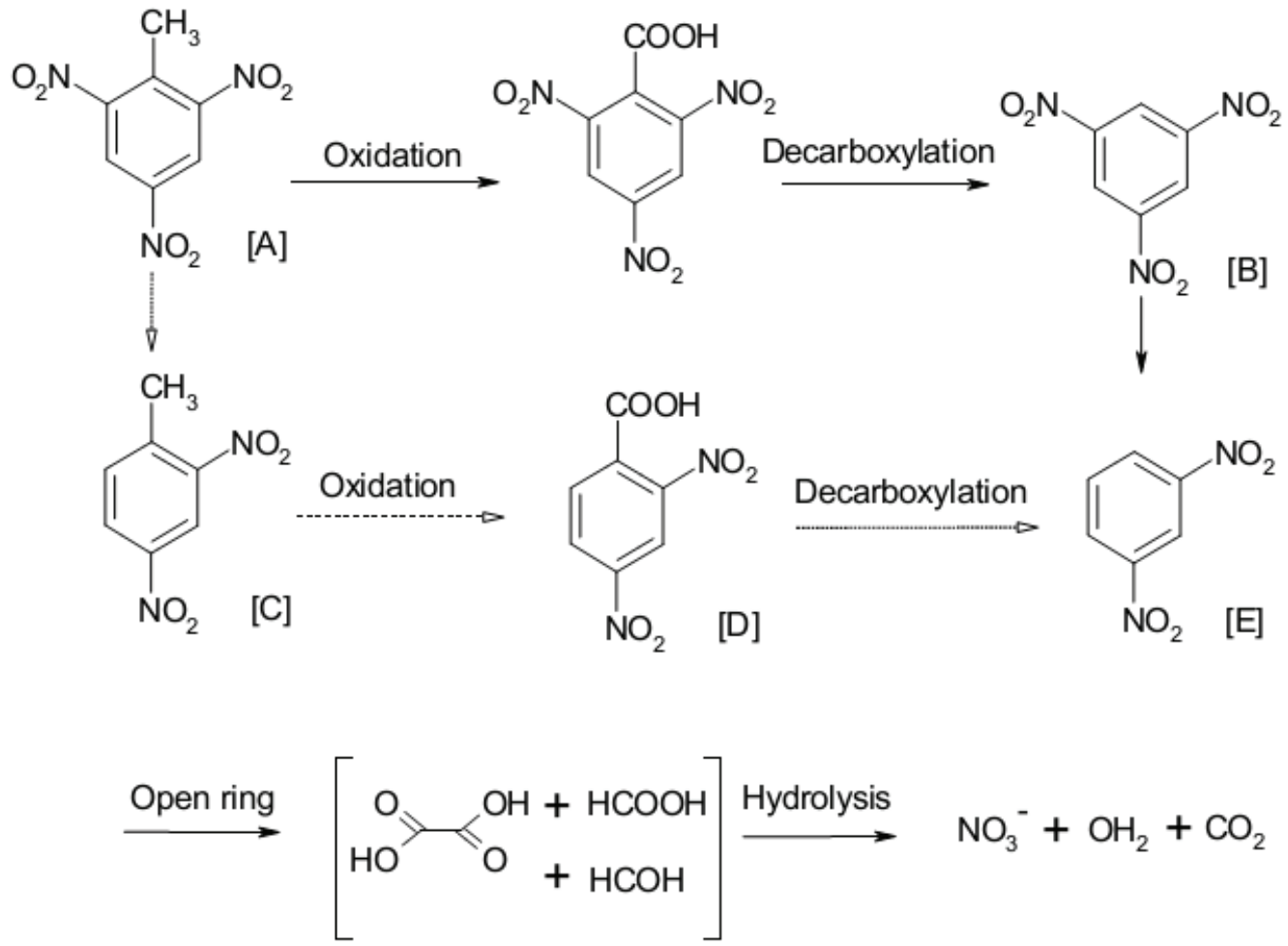

Scheme 1. The mechanism for the TNT decomposition as proposed by Liou et al. [49].

this level shows detrimental effects on the photodegradation of TNT [48].

The photocatalytic degradation mechanism of TNT was through oxidation of methyl group followed by decarboxylation of aromatic acid then mineralization of nitro groups. The final products of the cleavage of aromatic rings were formic and oxalic acids and nitrates. These by-products could be degraded gradually into final products of organic acids, water and carbon dioxide. Therefore, the degradation mechanism of photo-Fenton of TNT can be proposed as shown in Scheme 1.

4. Conclusions

Photocatalysis of the degradation of TNT using TiO_2 is shown to be enhanced by doping with iron up to 0.6 wt%. Parallel analysis by different characterization techniques (XRD, FTIR, UV–Vis and TEM) reveal that such an improvement is related to the effective introduction of Fe^{3+} ions in the TiO_2 structure. At higher iron content up to 0.8 wt%, the catalytic activity decreased mainly due to diffusion limitation in the catalyst pores, since the pore volumes of the 0.6 and 0.8 wt% Fe/TiO_2 catalysts are 0.2769 and 0.1541 cm^3/g, respectively.

Acknowledgments

We are indebted to the Egyptian Petroleum Research Institute (EPRI) who provided financial support of this research, which included the expenses of all analytical measurements

References

[1] D.I. Anwar, D. Mulyadi, Synthesis of Fe-TiO_2 composite as a photocatalyst for degradation of methylene blue, Procedia Chem., 17 (2015) 49–54.
[2] O. Ola, M.M. Maroto-Valer, Transition metal oxide based TiO_2 nanoparticles for visible light induced CO_2 photoreduction, Appl. Catal., A, 502 (2015) 114–121.
[3] E. Beyers, P. Cool, E.F. Vansant, Stabilisation of mesoporous TiO_2 by different bases influencing the photocatalytic activity, Microporous Mesoporous Mater., 99 (2007) 112–117.
[4] A.K. Aboul-Gheit, S.M. Ahmed, Homogeneous and heterogeneous kinetics of the photocatalytic degradation of hydrocarbons in water, Egypt. J. Pet., 10 (2001) 65–69.
[5] M.H. Zhou, J.G. Yu, B. Cheng, Effects of Fe-doping on the photocatalytic activity of mesoporous TiO_2 powders prepared by an ultrasonic method, J. Hazard. Mater., 137 (2006) 1838–1847.
[6] L. Haibin, L. Guocong, C. Shuguang, L. Qicheng, Novel Fe doped mesoporous TiO_2 microspheres: ultrasonic-hydrothermal synthesis, characterization, and photocatalytic properties, Physica E, 42 (2010) 1844–1849.

[7] L.G. Devi, N. Kottam, B. Narasimha Murthy, S.G. Kumar, Enhanced photocatalytic activity of transition metal ions Mn^{2+}, Ni^{2+} and Zn^{2+} doped polycrystalline titania for the degradation of Aniline Blue under UV/solar light, J. Mol. Catal. A: Chem., 328 (2010) 44–52.
[8] A.K. Aboul-Gheit, S.M. El-Sayed, S.M. Ahmed, Photocatalytic degradation of petroleum compounds from wastewater. Part 1: degradation of gas oil sing natural semiconductor catalyst, Egypt. J. Pet., 13 (2004) 17–21.
[9] G. Mamba, A. Mishra, Advances in magnetically separable photocatalysts: smart, recyclable materials for water pollution mitigation catalysts, Catalysts, 6 (2016) 79.
[10] Z. Li, W. Shen, W. He, X. Zu, Effect of Fe-doped TiO_2 nanoparticle derived from modified hydrothermal process on the photocatalytic degradation performance on methylene blue, J. Hazard. Mater., 155 (2008) 590–594.
[11] M. Khairy, W. Zakaria, Effect of metal-doping of TiO_2 nanoparticles on their photocatalytic activities toward removal of organic dyes, Egypt. J. Pet., 23 (2014) 419–426.
[12] A.K. Aboul-Gheit, D.S. El-Desouki, R.A. El-Salamony, Different outlet for preparing nano-TiO_2 catalysts for the photodegradation of Black B dye in water, Egypt. J. Pet., 23 (2014) 339–348.
[13] N. Kazumoto, F. Yuichi, M. Naoya, T. Toshiki, O. Teruhisa, Development of an S-doped titania nanotube (TNT) site-selectively loaded with iron(III) oxide and its photocatalytic activities, Appl. Catal., B, 84 (2008) 584–590.
[14] J. Treml, K. Smejkal, Flavonoids as potent scavengers of hydroxyl radicals, Compr. Rev. Food Sci. Food Saf., 15 (2016) 720–738.
[15] Z. Jia, J. Miao, H.B. Lu, D. Habibi, W.C. Zhang, L.C. Zhang, Photocatalytic degradation and absorption kinetics of cibacron brilliant yellow 3G-P by nanosized ZnO catalyst under solar light, J. Taiwan Inst. Chem. Eng., 60 (2016) 267–274.
[16] S. Kwon, M. Fan, A.T. Cooper, H. Yang, Photocatalytic applications of micro- and nano-TiO_2 in environmental engineering, Crit. Rev. Environ. Sci. Technol., 38 (2008) 197–226.
[17] S. Das, Photocatalytic nano-titanium dioxide for environmental application: an Overview, Int. J. Innovative Res. Sci. Eng. Technol., 5 (2016) 519–522.
[18] S. Kim, S. Hwang, W. Choi, Visible light active platinum-ion-doped TiO_2 photocatalys, J. Phys. Chem. B, 109 (2005) 24260–24267.
[19] Y. Liu, H. Wang, Z. Wu, Characterization of metal doped-titanium dioxide and behaviors on photocatalytic oxidation of nitrogen oxide, J. Environ. Sci., 19 (2007) 1505–1509.
[20] D. Liu, Y. Fernández, O. Ola, S. Mackintosh, M. Maroto-Valer, C.M.A. Parlett, A.F. Lee, J.C.S. Wu, On the impact of Cu dispersion on CO_2 photoreduction over Cu/TiO_2, Catal. Commun., 25 (2012) 78–82.
[21] J. Zhu, W. Zheng, B. He, J. Zhang, M. Anpo, Characterization of Fe–TiO_2 photocatalysts synthesized by hydrothermal method and their photocatalytic reactivity for photodegradation of XRG dye diluted in water, J. Mol. Catal. A: Chem., 216 (2004) 35–43.
[22] J.A. Navio, J.J. Testa, P. Djedjeian, J.R. Padron, D. Rodriguez, M.I. Litter, Iron-doped titania semiconductor powders prepared by a sol-gel method. Part II: photocatalytic properties, Appl. Catal., A, 178 (1999) 191–203.
[23] M.S. Nahar, K. Hasegawa, S. Kagaya, S. Kuroda, Comparative assessment of the efficiency of Fe doped TiO_2 prepared by two doping methods and photocatalytic degradation of phenol in domestic water suspensions, Sci. Technol. Adv. Mater., 8 (2007) 286–291.
[24] Y. Yang, C. Tian, Synergistic effects of sulfation and Fe-doping on the photocatalysis of titania, Res. Chem. Intermed., 36 (2010) 889–895.
[25] M. Kang, Synthesis of Fe/TiO_2 photocatalyst with nanometer size by solvothermal method and the effect of H_2O addition on structural stability and photodecomposition of methanol, J. Mol. Catal. A: Chem., 197 (2003) 173–183.
[26] R. Janes, L.J. Knightley, C.J. Harding, Structural and spectroscopic studies of iron (III) doped titania powders prepared by sol-gel synthesis and hydrothermal processing, Dyes Pigm., 62 (2004) 199–212.
[27] S.M. Abdel-Azim, A.K. Aboul-Gheit, S.M. Ahmed, D.S. El-Desouki, M.S.A. Abdel-Mottaleb, Preparation and application of mesoporous nanotitania photocatalysts using different templates and pH media, Int. J. Photoenergy, 2014 (2014) 1–11.
[28] A.M. Badawi, S.A. Shaban, S.M. Ahmed, S.M.I. Morsy, A.Y. El-Naggar, Kinetics of TNT degradation in the presence of zero valent iron nanocatalyst, Egypt. J. Chem., 55 (2012) 339–353.
[29] F.V. Santos, E.B. Azevedo, G.L. Sant'Anna Jr., M. Dezotti, Photocatalysis as a tertiary treatment for petroleum refinery wastewaters, Braz. J. Chem. Eng., 23 (2006) 451–460.
[30] A.K. Aboul-Gheit, S.M. Ahmed, D.S. El-Desouki, N.E. Moustafa, S.M. Abdel-Azeem, Nanocrystalline Pt/TiO_2 catalysts for 4-chlorophenol photocatalytic degradation, Egypt. J. Pet., 19 (2010) 45–58.
[31] P.P. Khirade, J.S. Kounsalye, A.R. Chavan, D. Sable, S.D. Birajdar, K.M. Jadhav, Effect of Fe^{3+} substitution on structural and magnetic properties of barium titanate nanoceramics, Bionano Front., 8 (2015) 154–156.
[32] R.D. Shannon, Revised effective ionic radii and systematic studies of interatomic distances in halides and chalcogenides, Acta Crystallogr., Sect. A, 32 (1976) 751–767.
[33] N. Šijakovic-Vujičić, M. Gotić, S. Musić, M. Ivanda, S. Popović, Synthesis and microstructural properties of Fe-TiO_2 nanocrystalline particles obtained by a modified sol-gel method, J. Sol-Gel Sci. Technol., 30 (2004) 5–19.
[34] O.Y. Wu, I.P. Parkin, G. Hyett, A neutron diffraction study of oxygen and nitrogen ordering in a kinetically stable orthorhombic iron doped titanium oxynitride, J. Solid State Chem., 190 (2012) 169–173.
[35] N. Toshima, T. Yonezawa, Bimetallic nanoparticles-novel materials for chemical and physical applications, New J. Chem., 22 (1998) 1179–1201.
[36] C.Y. Wang, D.W. Bahnemann, J.K. Dohrmann, A novel preparation of iron-doped TiO_2 nanoparticles with enhanced photocatalytic activity, Chem. Commun., 16 (2000) 1539–1540.
[37] M. Pelaez, N.T. Nolan, S.C. Pillai, M.K. Seery, P. Falaras, A.G. Kontos, P.S.M. Dunlope, J.W.J. Hamiltone, J.A. Byrnee, K. O'Sheaf, M.H. Entezari, D.D. Dionysiou, A review on the visible light active titanium dioxide photocatalysts for environmental applications, Appl. Catal., B, 125 (2012) 331–349.
[38] Y.H. Peng, G.F. Huang, W.Q. Huang, Visible-light absorption and photocatalytic activity of Cr-doped TiO_2 nanocrystal films, Adv. Powder Technol., 23 (2012) 8–12.
[39] Y. Wang, R. Zhang, J. Li, L. Li, S. Lin, First-principles study on transition metal-doped anatase TiO_2, Nanoscale Res. Lett., 9 (2014) 46–53.
[40] S.G. Kumar, L.G. Devi, Review on modified TiO_2 photocatalysis under UV/visible light: selected results and related mechanisms on interfacial charge carrier transfer dynamics, J. Phys. Chem. A, 115 (2011) 13211–13241.
[41] N.N. Mahamuni, A.B. Pandit, Effect of additives on ultrasonic degradation of phenol, Ultrason. Sonochem., 13 (2006) 165–174.
[42] J. Wang, Z. Jiang, L. Zhang, P. Kang, Y. Xie, Y. Lv, R. Xu, X. Zhang, Sonocatalytic degradation of some dyestuffs and comparison of catalytic activities of nano-sized TiO_2, nano-sized ZnO and composite TiO_2/ZnO powders under ultrasonic irradiation, Ultrason. Sonochem., 16 (2009) 225–231.
[43] A.D. Paola, G. Marcı, L. Palmisano, M. Sciavello, K. Uosaki, S. Ikeda, B. Ohtani, Preparation of polycrystalline TiO_2 photocatalysts impregnated with various transition metal ions: characterization and photocatalytic activity for the degradation of 4-nitrophenol, J. Phys. Chem. B, 106 (2002) 637–645.
[44] W. Choi, A. Termin, M.R. Hoffmann, The role of metal ion dopants in quantum-sized TiO_2: correlation between photoreactivity and charge carrier recombination dynamics, J. Phys. Chem., 98 (1994) 13669–13679.

[45] K.T. Ranjit, B. Viswanathan, Synthesis, characterization and photocatalytic properties of iron-doped TiO_2 catalysts, J. Photochem. Photobiol., A, 108 (1997) 79–84.
[46] P. Kokila1, V. Senthilkumar, K. PremNazeer, Preparation and photocatalytic activity of Fe^{3+}-doped TiO_2 nanoparticles, Arch. Phys. Res., 2 (2011) 246–253.
[47] M. Zhou, J. Yu, B. Cheng, H. Yu, Preparation and photocatalytic activity of Fe-doped mesoporous titanium dioxide nanocrystalline photocatalysts, Mater. Chem. Phys., 93 (2005) 159–163.
[48] K. Naeem, F. Ouyang, Preparation of Fe^{3+}-doped TiO_2 nanoparticles and its photocatalytic activity under UV light, Physica B, 405 (2010) 221–226.
[49] M.J. Liou, M.C. Lu, J.N. Chen, Oxidation of TNT by photo-Fenton process, Chemosphere, 57 (2004) 1107–1114.